CHEMISTRY OF MATERIALS

pubs.acs.org/cm

Article

Improving Charge Transfer in Metal−Organic Frameworks through Open Site Functionalization and Porosity Selection for Li−S Batteries

Bingqian Liu and V. Sara Thoi*

Cite This: *Chem. Mater.* 2020, 32, 8450−8459

Read Online

ACCESS | Metrics & More | Article Recommendations | Supporting Information

ABSTRACT: The tunable nature of metal−organic frameworks (MOFs) enables versatility and precise control over structures and properties, making them feasible for potential applications including gas storage and separation, catalysis, molecular sensing, and energy storage. However, porous MOFs are typically insulating, greatly limiting their utility in electrochemical devices. Introducing redox activity to MOFs can promote charge conduction and provide insights into redox mechanisms in a multidimensional coordination system. Toward this end, we prepared a series of anthraquinone (AQ)-functionalized zirconium MOFs (MOF-AQ) to investigate the relationship between porosity and charge transfer reactions using the canonical MOF-808 and NU-1000 frameworks. We evaluated the ability of these frameworks as sulfur host materials to promote polysulfide redox, which are critical conversions for Li−S batteries. Li−S batteries are promising contenders as high-capacity energy storage devices, with an energy density surpassing that of Li ion batteries. We found that the incorporation of AQ on the nodal structure leads to improvement in specific capacity, particularly at high charge and discharge rates. More importantly, enhanced electrochemical behavior of NU-1000-AQ over MOF-808-AQ suggests that larger pore aperture favors overall charge transfer and diffusion. Our study demonstrates there is a delicate balance between AQ loading and available pore volume for ion flux to achieve optimized charge transfer efficiency under fast charge−discharge conditions. Our work provides insight for future designs of novel redox-active MOFs to facilitate charge transport in porous coordination networks.

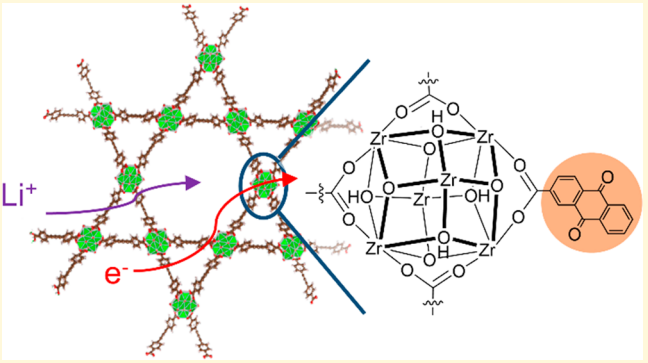

INTRODUCTION

Metal−organic frameworks (MOFs) are a class of porous crystalline hybrid materials composed of inorganic nodes and organic linkers. The versatile selection and combination of nodes and linkers permit precise control over their chemical and structural properties, such as porosity, stability, and particle morphology. The modular nature of MOFs makes them promising candidates for advanced electrochemical devices.[1−4] Lithium−sulfur (Li−S) batteries have gained widespread attention with their high theoretical specific capacity (1675 mAh g^{-1}), environmental benignity, and low cost.[5,6] Despite the great potentials as next-generation energy storage devices, Li−S batteries still face major technical challenges. In a typical discharging process, sulfur (S_8) is first reduced to soluble lithium polysulfides (Li_2S_x, $x = 4−8$) before terminating at insoluble lithium sulfide (Li_2S). Generated polysulfides can leach into the electrolyte and migrate from cathode to anode, causing the well-known "shuttle effect" that leads to active material loss and electrode surface passivation.[7,8] Additionally, the large volume expansion upon lithiation for sulfur can cause cathode pulverization and sulfur isolation.[7] Because of the aforementioned aspects, Li−S batteries suffer from rapid capacity decay, high self-discharging rate, and safety issues. Such challenges can be overcome by adopting a porous matrix as a sulfur host. With their highly porous nature and facile tunability, MOF hosts are effective in polysulfide encapsulation.[3,9,10]

It is important to note that electronic and ionic transport are crucial in Li−S batteries. However, MOFs are usually insulating due to the strong interactions between hard transition metal ions and hard oxygen atoms from redox-inactive carboxylic acid linkers.[11] Modulating charge transport in MOFs is thus of great importance to mitigate their limitations as effective materials for electrochemical applications. Some recent works have focused on improving electrical conductivity utilizing MOF composites as sulfur hosts.[12−16] Redox-active MOFs are particularly interesting since they can

Received: June 10, 2020
Revised: September 4, 2020
Published: September 4, 2020

https://dx.doi.org/10.1021/acs.chemmater.0c02438
Chem. Mater. 2020, 32, 8450−8459

offer opportunities to gain fundamental insights into charge transfer mechanism in a multidimensional coordination space.[11,17,18] The redox activity of MOFs can be generated from either the existence of redox-active components (metal centers or ligands) in the framework or the introduction of redox-active species postsynthetically (through covalent bonding or impregnation as guests).[19−22] There has been increasing interest in illuminating the relationship between the MOF structure and charge transport and diffusion.[9,23] As previously studied, electron transfer in MOFs usually happens through redox hopping, accompanied by ion diffusion.[24] Thus, MOF porosity plays an important role in the charge transfer rate and efficiency as it affects electron hopping distance and ion flux simultaneously. Larger pores facilitate ion movement while slowing down electron hopping. Ferrocene incorporated MOFs with various pore apertures were utilized to unveil this delicate balance, demonstrating ion diffusion is the rate-limiting process and larger pores render higher overall charge transfer rate constant.[25−30] Inspired by these works, we adopted functionalized MOFs as sulfur hosts and evaluated the effect of redox-active components as well as porosity on charge transport and diffusion in Li−S batteries.

Herein, we selected zirconium MOFs, MOF-808 and NU-1000, as the platform because of their extraordinary chemical stability and accessible open sites for functionalization.[31] We, and others, have previously fabricated redox-active MOFs utilizing anthraquinone (AQ)-based linkers since these moieties can undergo reversible redox reactions to store two electrons.[32−34] In the present work, we installed redox-active AQ sites in MOF-808 and NU-1000 postsynthetically at the Zr node by substituting redox-innocent carboxylate ligands with anthraquinone-2-carboxylic acid (AQ-COOH). Compared to utilizing AQ-based linkers as building blocks,[32−34] postsynthetic incorporation at the metal cluster enables tunability and selection over desired loading amount and pore structure. With the prediction that AQ incorporation leads to enhanced charge mobility and boosted local lithium ion concentration during cycling, increasing loading amount would further facilitate charge transfer and polysulfide redox. On the other hand, we also expect more blocked and crowded pore environments with higher AQ loading, which may dampen ion flux for fast charge−discharge. Our work investigates into this balance between charge transport and porosity in MOF-AQ in the context of sulfur redox and Li−S batteries.

EXPERIMENTAL SECTION

General. All chemicals were used as received without further purification. MOF and MOF-AQ samples were analyzed by using powder X-ray diffraction (PXRD, Bruker D8 Focus diffractometer, Cu Kα, LynxEye detector) and Fourier transform infrared spectroscopy (IR, ThermoScientific Nicolet iS FT-IR with iD 5 ATR attachment). Thermogravimetric analysis (TGA) was conducted using a TA Instruments SDT Q600 under flowing Ar at a heating rate of 5.0 °C min^{-1}. Nitrogen adsorption isotherms (Micromeritics ASAP 2020) were collected on samples to calculate surface areas and pore volumes. The Brunauer−Emmett−Teller (BET) method was applied to obtain a surface area from the N_2 adsorption isotherms.

Synthesis of NU-1000-AQ. NU-1000 was synthesized following previously reported procedures.[35] As-synthesized NU-1000 powder was washed with DMF and acetone before dried under vacuum. Anthraquinone−2−carboxylic acid (AQ−COOH) was incorporated into NU-1000 by solvent-assisted ligand incorporation (SALI) treatment.[36] AQ−COOH (112 mg, 0.44 mmol) was fully dissolved in DMF before NU-1000 (200 mg) was added to the solution. The resulting suspension was set at room temperature for 1 day with occasional swirling. Anthraquinone-functionalized MOF was collected by centrifugation and washed with DMF (3 × 20 mL) over 3 days and then with acetone (3 × 20 mL) over 3 days. The resulting NU-1000-AQ was dried under vacuum for 3 h for further characterization.

Synthesis of MOF-808-xAQ. MOF-808 was synthesized following previously reported procedures.[37] As-synthesized MOF-808 powder was washed with DMF and acetone before dried under vacuum. For the synthesis of MOF-808-3xAQ, excess AQ−COOH (232 mg, 0.92 mmol) was fully dissolved in DMF before 200 mg of MOF-808 was added to the solution. For the synthesis of MOF-808-1.5xAQ, AQ−COOH (51.8 mg, 0.21 mmol) was first dissolved in DMF before mixing with MOF-808 (200 mg). After soaking at room temperature for 1 day, the precursor solution was decanted. MOF-808-xAQ samples were further washed with DMF (3 × 20 mL) over 3 days and then with acetone (3 × 20 mL) over 3 days. Resulting anthraquinone-loaded MOF-808 powders were collected by centrifugation and dried under vacuum for 3 h for further characterization.

Quantification of AQ-COOH in MOF-AQs. The loading amount of anthraquinone carboxylate in MOF-AQ was determined by nuclear magnetic resonance (NMR) spectroscopy. ^{1}H NMR spectra were collected using a 400 MHz Bruker Avance II spectrometer. Samples were prepared by digesting ∼5 mg of MOF-AQ powder in 10% D_2SO_4/d_6-DMSO solution for 24 h. There are 3, 22, and 7 protons (excluding protons on carboxylic acid groups) respectively in one molecule of H_3BTC (linker for MOF-808), H_4TBAPy (linker for NU-1000), and AQ-COOH. For both MOFs, the node/ligand ratio is 1:2. Therefore, the ratio of AQ vs node is determined by the following calculation:

$$\text{NU-1000-AQ: } \frac{\frac{\text{Intergration of AQ}}{7}}{\frac{\text{Intergration of H4TBAPy linker}}{22}} \times 2$$

$$\text{MOF-808-xAQ: } \frac{\frac{\text{Intergration of AQ}}{7}}{\frac{\text{Intergration of H3BTC linker}}{3}} \times 2$$

Cathode and Coin Cell Preparation. All MOF and MOF-AQ powders were activated at ∼150 °C for 3 h under vacuum to remove the solvent guest molecules in the pores before cathode preparation. The cathode slurry for cell cycling was prepared by using a 30 wt % MOF, 45 wt % S (Sigma-Aldrich), 15 wt % Super-P carbon (99+%, Alfa Aesar), and 10 wt % poly(vinylidene fluoride) (PVDF, Alfa Aesar) solid mixture in *N*-methyl-2-pyrrolidinone (NMP, Oakwood Chemical). The MOF was first ground with a mortar and pestle and then mixed with sulfur. PVDF, Super-P carbon, and a small stainless-steel ball were added to the mixture, and the solids were vortexed for 5 min. The slurry was formed by adding NMP to the solid mixture and thoroughly mixed on the vortex mixer for at least 30 min. Once homogenized, the slurry was cast onto preweighed 12.7 mm carbon paper disks and dried overnight in an 80 °C oven. The 12.7 mm cathodes were weighed again to determine the sulfur loading and stored in an Ar-filled glovebox until use. Cathodes without added sulfur were prepared for investigating the redox behavior and electrochemical contribution of MOF-AQ by using a similar procedure, containing 30 wt % MOF, 50 wt % Super-P carbon, and 20 wt % PVDF. The control cathode slurry consisting of the physical mixture of MOF-808 and AQ-COOH was prepared by using 30 wt % MOF, 15 wt % AQ-COOH, 40 wt % Super-P carbon, and 15 wt % PVDF.

CR 2032-type coin cells were constructed in an Ar-filled glovebox using a preweighed cathode, a polished metallic Li anode, two Celgard separators, and two stainless steel spacers and spring (TOB New Energy). The electrolyte was composed of 1.0 M bis(trifluoromethanesulfonyl)imide lithium (LiTFSI, Oakwood Chemical) in a mixed solution of 1,2-dimethoxyethane (DME, 99+%, Alfa Aesar) and 1,3-dioxolane (DOL, 99.5%, Acros Organics) (1:1, v/v) with an added 2 wt % lithium nitrate salt ($LiNO_3$, 99%, Strem Chemicals). To ensure reproducibility, the amount of electrolyte added to each coin

https://dx.doi.org/10.1021/acs.chemmater.0c02438
Chem. Mater. 2020, 32, 8450−8459

Scheme 1. Structures of Pristine NU-1000[35] and MOF-808[37]

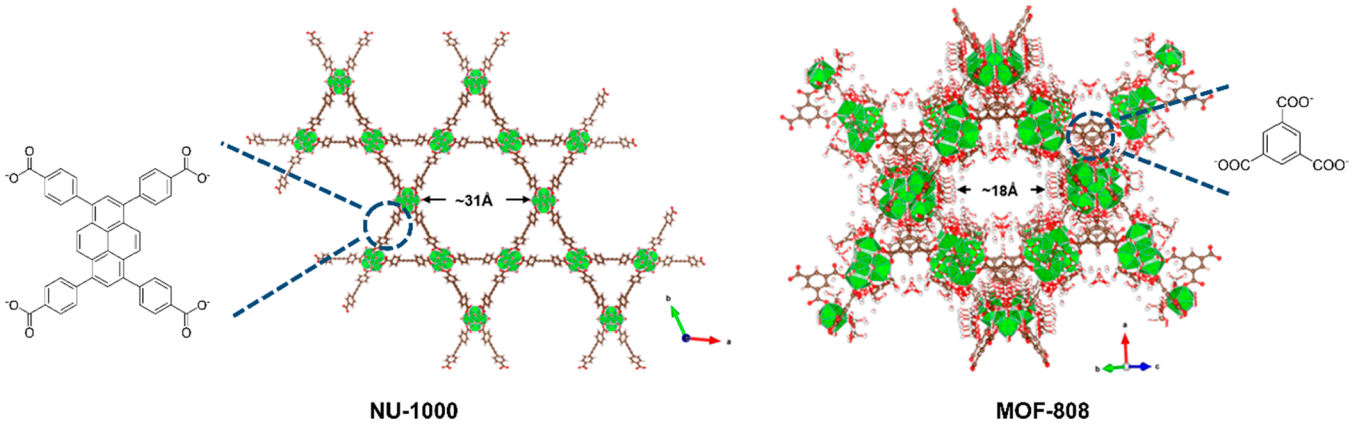

Scheme 2. Solvent-Assisted Ligand Incorporation Treatment to Substitute Bound Modulators with AQ-COOH[a]

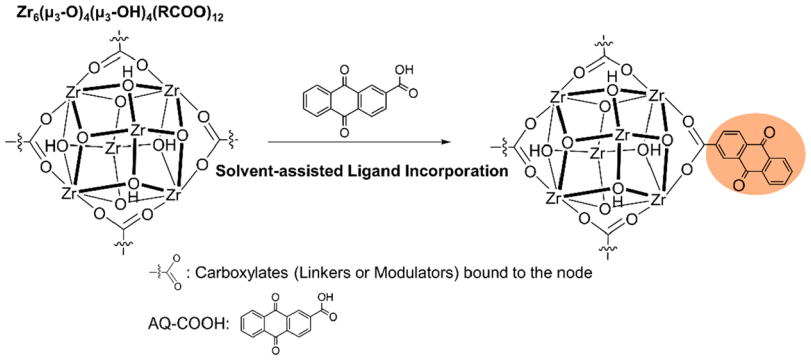

[a]Only 1/3 of the carboxylates are shown for simplicity.

cell assembly was normalized to the mass of S on the cathode with the ratio of 60 μL per mg of S.

Electrochemical Analysis. Cyclic voltammetry (CV) was performed on an Ivium-n-STAT multichannel electrochemical analyzer. Freshly prepared coin cells with MOF-AQ composite cathodes and control cathodes were cycled between 2.7 and 1.8 V vs Li/Li^+ to examine their electrochemical property. Cells were cycled galvanostatically (MNT-BA-5 V, MicroNanoTools) after resting for 8 h. For long-term cycling, cells were cycled at a *C*-rate of *C*/10 for the first cycle, followed by 100 cycles at *C*/2. At least three cells were tested under the same conditions for these experiments. For the rate capability test, cells were cycled at the rate of *C*/2, 1*C*, 2*C*, 3*C*, and 4*C* for five cycles followed by 20 cycles at *C*/2. Electrochemical impedance spectra (EIS) were collected by using an Ivium-n-STAT multichannel electrochemical analyzer on the cells in the discharged state after the last cycle, and the data was processed by using Iviumsoft. The spectra were modeled by an equivalent circuit of R_1–R_2//CPE_1-R_3(W_1)//CPE_2, where R_1 is the electrolyte resistance, R_2 is the resistance from the insulating species deposited on both electrodes, R_3 is the charge transfer resistance, and W_1 is the Warburg element.[38]

RESULTS AND DISCUSSION

Materials Synthesis and Characterization. Two types of Zr MOF with different pore sizes and open sites, MOF-808 and NU-1000, were synthesized by a previously reported solvothermal method.[35,37] NU-1000 has 8-connected nodes, leading to four open sites and two kinds of pores with sizes of 12 and 31 Å (Scheme 1).[35] MOF-808 has 6-connected Zr nodes, resulting in six open sites and two kinds of cages: a tetrahedral cage with pore diameter of 4.8 Å and an adamantane cage with pore diameter of 18.4 Å.[37] Redox activity was introduced to as-synthesized MOFs by the solvent-assisted ligand incorporation (SALI) method (Scheme 2). AQ-COOH was successfully grafted onto MOFs by substituting the labile redox-innocent monocarboxylates (such as formates and benzoates, known as modulators[39]) bound to the Zr node. The loading content per Zr_6 node in these AQ functionalized MOF (MOF-AQ) samples can be tuned by the amount of ligand added in the SALI procedure. The ratio of anthraquinone carboxylate to Zr_6 node was determined by ^{1}H NMR analysis of digested MOF-AQ samples (Figure S1). For NU-1000-AQ, the ratio of AQ to Zr_6 node is approximately 4:1, suggesting all available Zr sites were functionalized (34.4 wt % AQ calculated). A different AQ loading amount was achieved in MOF-808 (MOF-808-*x*AQ, *x* represents the ratio of incorporated AQ to Zr_6 node), where MOF-808-3*x*AQ contains 38.1 wt % AQ and MOF-808-1.5*x*AQ consists of 22.6 wt % AQ (Table S1). Interestingly, no more than 3 equiv of AQ per Zr_6 node can be incorporated in MOF-808 under the same SALI procedures even if a great excess of AQ-COOH was added. The different maximum amounts of AQ in NU-1000 and MOF-808 suggest the AQ loading efficiency relies on the number of open sites and pore size simultaneously.

The functionalized MOFs were characterized by powder X-ray diffraction (PXRD), infrared spectroscopy (IR), thermogravimetric analysis (TGA), and Brunauer–Emmett–Teller (BET) surface area analysis. Similar PXRD patterns of MOF-AQ and pristine MOF confirm the frameworks are structurally intact after SALI treatment (Figure S2). Three peaks for C=O stretching band in AQ-COOH are seen in the IR; the band at

https://dx.doi.org/10.1021/acs.chemmater.0c02438
Chem. Mater. 2020, 32, 8450–8459

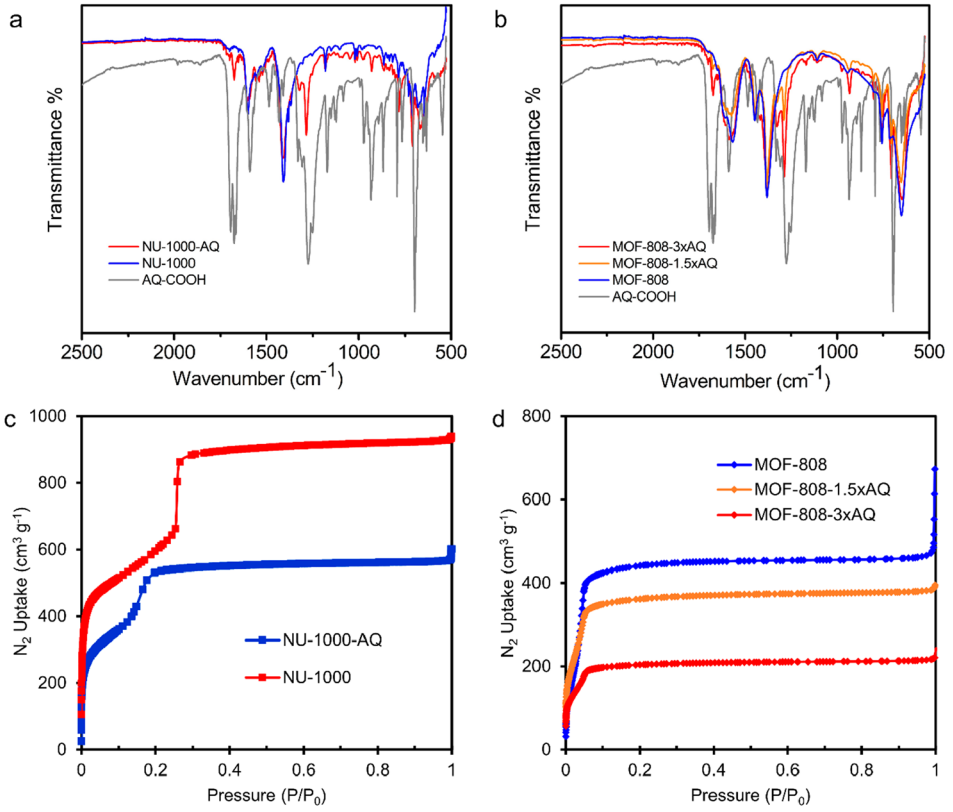

Figure 1. IR spectra of (a) NU-1000 and (b) MOF-808 before and after functionalization. Nitrogen adsorption isotherms of (c) NU-1000, NU-1000-AQ, and (d) MOF-808, MOF-808-*x*AQ samples.

1695 cm^{-1} is attributed to the C═O stretch of the carboxylic acid,[40] and 1675 and 1665 cm^{-1} are assigned to the C═O stretches from the two asymmetric ketone groups in the anthraquinone core (Figure 1a,b). In MOF-AQs, the C═O stretch from the carboxylic acid disappears as anticipated since the band for a Zr-bound AQ carboxylate should have similar absorption as that of the linker-based Zr-carboxylate at around 1600 and 1400 cm^{-1}.[41] The C═O stretches from the ketone groups are seen as a single band in all MOF-AQs, with higher intensity observed with increasing AQ loading in MOF-808. Thermal stability of MOF-AQ was examined by TGA (Figure S3). In both cases, MOF-AQ starts to decompose at a slightly lower temperature compared to pristine MOF with the degradation temperature decreasing with increasing AQ incorporation. Finally, nitrogen adsorption isotherms measured at 77K (Figure 1c,d) illustrate the incorporation of AQ leads to decreased BET surface area and reduced pore volume. As shown in MOF-808-*x*AQ series, surface area and pore volume also decrease as a function of increasing AQ loading (Table S2), consistent with the occupation of pore space in the framework by the anthraquinone moiety. The pore size distribution of NU-1000-AQ and MOF-808-3*x*AQ demonstrate similar shifts compared to their parent MOFs (Figure S4). The values of pore size drop in both MOFs indicate not all AQ are directly pointing at the pore center.

The incorporation of AQ into the MOFs was also demonstrated electrochemically. Composite electrodes consisting of MOF-AQ, Super P carbon, and poly(vinylidene fluoride) (PVDF) were constructed for cyclic voltammetry (CV). Cyclic voltammograms of NU-1000-AQ and MOF-808-3*x*AQ show two pairs of redox features corresponding to the two one-electron redox reaction from the anchored anthraquinone species[42] and illustrate the AQ motif is electrochemically accessible despite the insulating nature of the framework (Figure 2a). The half-wave potentials ($E_{1/2}$) are 2.24 and 2.40 V (vs Li/Li^+) in NU-1000-AQ and 2.23 and 2.38 V (vs Li/Li^+) in MOF-808-3*x*AQ. The slight anodic shift in the reduction potential in NU-1000-AQ relative to MOF-808-3*x*AQ suggests that the AQ moieties are easier to reduce in the larger channels of NU-1000 compared to those of MOF-808. Additionally, peak currents of both MOFs have a linear dependence on square root of scan rates (Figure S5 and Figure 2c,d), demonstrating that charge hopping is diffusion-controlled despite being in a solid matrix.[25] To confirm that the AQ-COOH moieties have infiltrated into the porous framework, a mixture of MOF-808 and AQ-COOH was constructed into an analogous composite electrode (Figure 2b). The physically mixed MOF and AQ-COOH composite electrode shows obvious cathodically shifted reduction potentials and increased peak-to-peak separations, illustrating that the nongrafted AQ moiety is less electrochemically active.

Li−S Cycling Performance and Analysis. A Li anode and a composite cathode containing a physical mixture of 30 wt % MOF, 45 wt % S, 15 wt % Super P carbon, and 10 wt % PVDF were assembled into a CR 2032-type coin cell. Based on previous studies, sulfur is reduced to polysulfides during the discharge cycle and the dissolved polysulfides subsequently diffuse into the MOF pores.[43,44] To confirm, MOF-808-AQ powder is soaked in a polysulfide solution (10 mM Li_2S_6 in 1:1 DOL/DME) for 24 h. The color of the solution turned from orange to transparent (Figure S6), indicating the polysulfides have diffused into the MOF pores. UV−vis spectra of

https://dx.doi.org/10.1021/acs.chemmater.0c02438
Chem. Mater. 2020, 32, 8450−8459

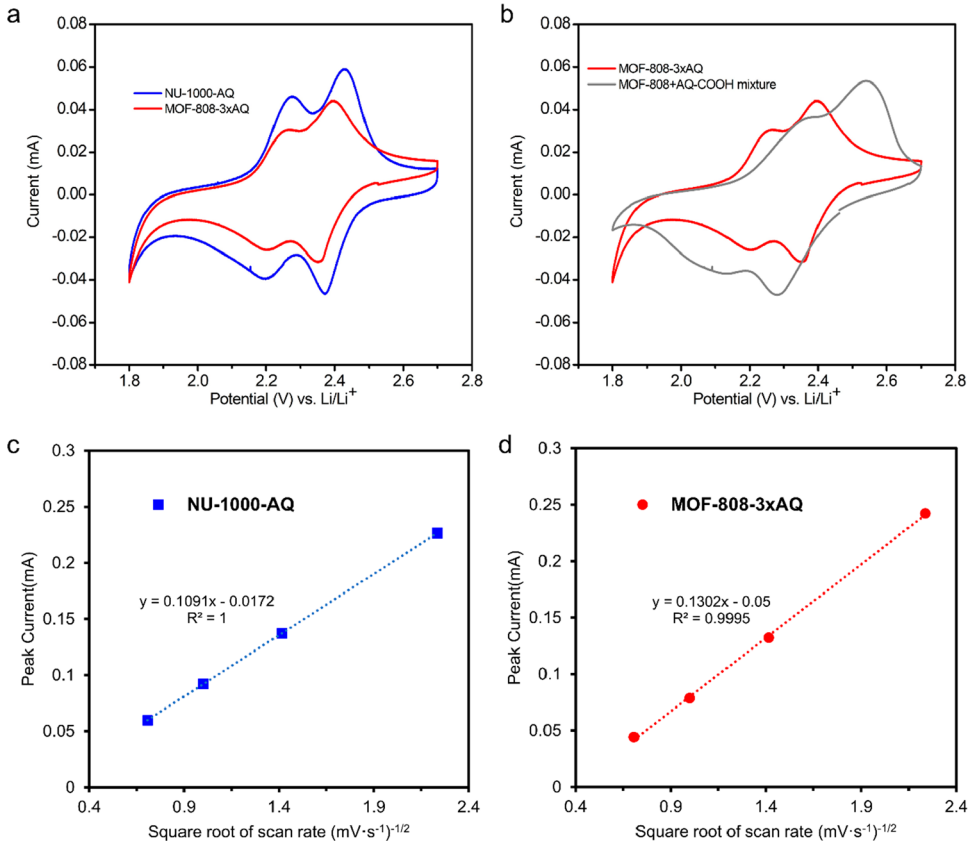

Figure 2. Cyclic voltammograms of (a) NU-1000-AQ and MOF-808-3*x*AQ and (b) MOF-808-3*x*AQ and MOF-808+AQ-COOH mixture. Linear fit of peak current dependence on square root of scan rate for (c) NU-1000-AQ and (d) MOF-808-3*x*AQ.

Li_2S_6solution before and after soaking with MOF-808-AQ are shown in Figure S7. The disappearance of S_6^{2-}peak (around 350 nm)[45,46] in the supernatant demonstrates that MOFs possess the ability to uptake lithium polysulfides from solution.

Impact of AQ Loading in NU-1000. The electrochemical behavior of these "MOF+S" composites was first examined by CV cycled at various scan rates. NU-1000 and NU-1000-AQ cells both show two reduction peaks and an oxidation peak, as expected for typical Li−S cycling (Figure S8). The two cathodic events correspond to the two-stage reduction from S_8 to polysulfide (Li_2S_x) and Li_2S_x to Li_2S. Sulfur mass-normalized peak current plotted as a function of the square root of scan rate shows a linear dependence, confirming that the charge transfer during cycling are diffusion-controlled (Figure 3a,b). The slope of the linear fits can be used as a proxy for the diffusion coefficient according to the Cottrell equation.[47] The NU-1000-AQ+S composite cathode has an increased slope in both steps compared to NU-1000+S, suggesting AQ incorporation promotes diffusion of electroactive species.

Subsequently, the performance of MOF+S composite cathodes was examined by galvanostatic charging−discharging over the voltage range of 1.6−2.9 V (vs Li/Li^+). Long-term cycling at the rate of C/2 (fully charge/discharge in 2 h) was investigated and presented in Figure 3c. We note that cell-to-cell variation is common in battery cycling because of slight differences in electrolyte volume, error in cathode component masses, and internal cell pressure; thus, all long-term cycling data are shown for triplicate cells. NU-1000-AQ+S cells exhibit excellent performance with enhanced specific capacity and capacity retention compared to NU-1000+S. NU-1000-AQ composite cathodes deliver an average capacity of 693 mAh g^{-1} after 100 cycles with a high capacity retention of 86%. In comparison, NU-1000+S only retains 75% of the initial capacity at the 100th cycle with a final capacity of 540 mAh g^{-1}, a 22% decrease compared to that of NU-1000-AQ+S.

The rate capability of composite cathodes was also investigated by cycling at various *C* rates (Figure 3d and Figure S9). High discharge capacities are observed for NU-1000-AQ+S cathodes, reaching 885, 769, 640, 553, and 453 mAh g^{-1} at the last cycle of *C*/2, 1*C*, 2*C*, 3*C*, and 4*C*, respectively. When cycling back to the moderate rate of *C*/2, NU-1000-AQ+S was able to recover and stabilize around 820 mAh g^{-1}. In contrast, NU-1000+S exhibits a larger capacity fade as the *C* rate increases, only delivering a capacity of 365 mAh g^{-1} at 4*C*. NU-1000-AQ+S demonstrates higher capacity over NU-1000+S at all *C* rates and improved capacity retention at high rates. The impressive rate capability of NU-1000-AQ+S enables potential application in fast charge−discharge devices. Control experiments were also performed under the same cycling range and rates by using an NU-1000-AQ composite cathode without sulfur. As shown in Figure S10, the NU-1000-AQ host provides negligible contribution to the capacity, ruling out the possibility that the improvement mainly originates from extra charge storage of AQ.

Galvanostatic profiles and electrochemical impedance spectroscopy (EIS) were investigated to better understand the enhancement of NU-1000-AQ+S composite cathodes. Figure 4a shows the typical charge−discharge profile for NU-1000+S and NU-1000-AQ+S at *C*/2. They both exhibit the two characteristic plateaus for sulfur reduction at around 2.3 and 2.0 V (vs Li/Li^+) in the discharging process. The upper voltage plateau corresponds to the reduction of S_8 to soluble Li_2S_x,

https://dx.doi.org/10.1021/acs.chemmater.0c02438
Chem. Mater. 2020, 32, 8450−8459

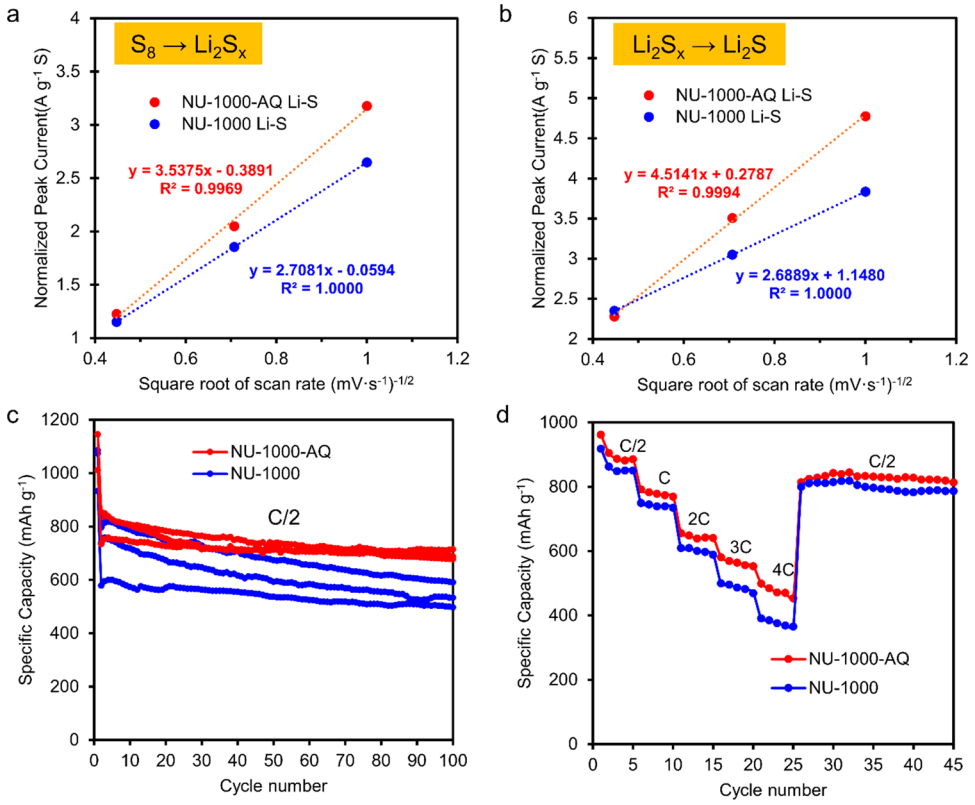

Figure 3. Impact of AQ loading on electrochemical behavior in Li−S cells. (a, b) Scan rate dependence plot. Sulfur mass-normalized peak current was plotted as a function of the square root of scan rate for the two-stage reduction of MOF+S composites, (c) galvanostatic cycling of NU-1000 and NU-1000-AQ at 1 × *C*/10 and 99 × *C*/2 (shown for triplicate cells), and (d) galvanostatic cycling results of NU-1000 and NU-1000-AQ at various charging−discharging rates.

while the lower plateau results from the reduction of long-chain polysulfides to insoluble Li_2S_2 and Li_2S. The voltage difference (ΔV) between charge and discharge curves is similar at all states for both composites, suggesting that AQ loading does not change the discharge mechanism and polysulfide equilibrium pathways at *C*/2. Notably, NU-1000-AQ+S composites demonstrate more defined plateaus and less sloping curves at higher rates compared to NU-1000+S (Figure 4b, Figure S11 and S12). They also exhibit a smaller ΔV starting from 2*C* (Table S3), suggesting AQ functionalization can facilitate polysulfide equilibria and reduce the overpotential for fast charge and discharge. These results further validate the advanced ion diffusion and electrochemical accessibility to polysulfide species of NU-1000-AQ+S composites.

To discern the charge transfer kinetics, EIS measurements were conducted on cells in their fully discharged state after 100 cycles at *C*/2 (Figure 4c and Table S4) and after the rate capability test (Figure S13 and Table S5). NU-1000-AQ+S cells exhibit lower electrode surfaces resistance (*R*2), charge transfer resistance (*R*3), and Warburg impedance (*W*) in both cases.[38] The lower *R*2 results from less insulating species deposited on the electrode surface, confirming addition of AQ mitigates surface passivation by reducing polysulfide leaching. The decreased value of *R*3 further validates faster redox kinetics of NU-1000-AQ+S, which favors high ion flux. Warburg impedance of NU-1000-AQ+S and NU-1000+S cells cycled for rate capability tests demonstrates a greater difference than those cycled at *C*/2, illustrating larger diffusion limitations in nonfunctionalized MOF host at high *C* rates. On the basis of these results, we ascribe the superior cyclability and higher charge transfer efficiency of NU-1000-AQ+S to the incorporation of AQ moiety. The loaded AQ species can undergo Li^+-coupled redox conversion, providing additional redox-active sites for mobilizing charges and boosting local Li^+ concentration. The increased Li^+ concentration also leads to stronger interactions with negatively charged polysulfides, which can further mitigate their leaching into the electrolyte.

Impact of Porosity. It has been shown previously that pore geometry is critical since hopping distances and pore apertures for ion flux determine charge transfer efficiency.[9] To study the impact of porosity on electrochemical behavior of MOF-AQ+S composites, MOF-808 was selected to compare with NU-1000 because of its much smaller pore windows. Upon functionalization, pore volume and BET surface area of MOF-AQs are greatly reduced compared to the pristine MOFs, confirming that AQ occupies pore space significantly. Cycling performance of cells with MOF-808-3*x*AQ and NU-1000-AQ additives (Figure 5a,b and Figure S14) were compared since they have similar gravimetric loading amount of AQ but distinct pore apertures and pore volumes. MOF-808-3*x*AQ+S cathodes demonstrate worse rate capability with much lower capacity at all *C* rates, only retaining a capacity of 320 mAh g^{-1} at the last cycle of 4*C*, which is 29% less than that of NU-1000-AQ+S. Galvanostatic profiles (Figures S15 and S16) of cells cycled at various *C* rates confirm their different behaviors. With less defined second plateaus, more sloping curves, and larger ΔV, MOF-808-3*x*AQ features inferior ion diffusion and polysulfide equilibria than NU-1000-AQ. The worse sulfur utilization of MOF-808-3*x*AQ+S can be ascribed to their smaller pore

https://dx.doi.org/10.1021/acs.chemmater.0c02438
Chem. Mater. 2020, 32, 8450−8459

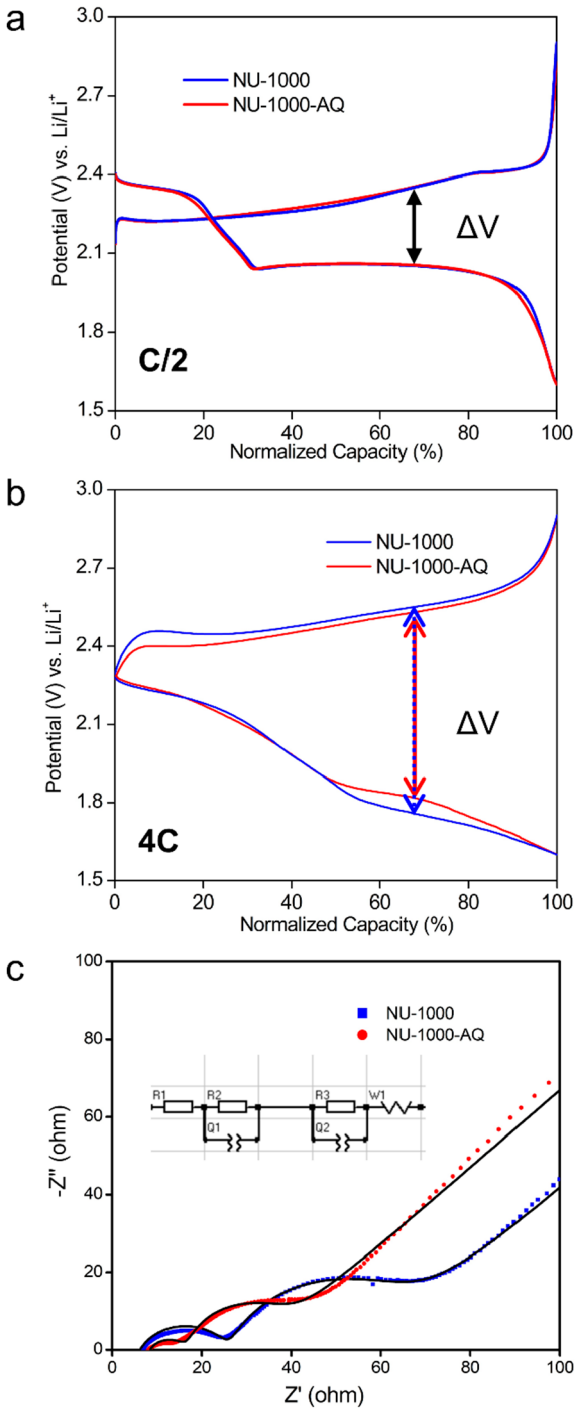

Figure 4. Normalized galvanostatic profiles of NU-1000+S and NU-1000-AQ+S at (a) *C*/2 and (b) 4*C* and (c) EIS and fitting curves (black line) collected on coin cells after 100 cycles at *C*/2 in the discharged state. The model circuit is shown as the inset.

aperture available for ion diffusion since less ions can pass through for a given time compared to NU-1000-AQ. Additionally, long-term cycling at *C*/2 and rate capability up to 4*C* were compared for MOF-808+S and NU-1000+S composites as a control (Figure S17). Similarly, NU-1000+S cathodes show higher capacity at all *C* rates. It is noteworthy that the differences in capacity and retention between two pristine MOF composites are less than that of AQ functionalized ones, confirming that pore aperture and AQ incorporation both play important roles in affecting electrochemical performance. On the basis of these results, we postulate that MOFs with larger pore aperture are more suitable for cycling at high charge and discharge rates.

Our electrochemical findings reveal the contrasting role of AQ. While AQ incorporation results in enhanced electrochemical accessibility of polysulfide species and faster redox kinetics, it can also partially block the pores for high ion flux. Because pore channels are also critical for ion transfer, a balance between AQ loading and available pore volume must be achieved to optimize charge transfer in Li−S batteries. To test this hypothesis, we utilized MOF-808 as a platform to investigate the effect of AQ loading by comparing MOF-808-1.5*x*AQ and MOF-808-3*x*AQ. As confirmed by ^{1}H NMR and BET analysis, MOF-808-1.5*x*AQ has less equivalents of AQ incorporated and a larger pore volume compared to MOF-808-3*x*AQ. Redox properties of MOF-808-*x*AQ+S composites are revealed in CV (Figure S18) over the range of 1.6−2.9 V (vs Li/Li^{+}). Both composites show the typical two cathodic events and one broad anodic event. The linear dependence of peak currents on the square root of scan rates suggests that charge transfer of electroactive species is diffusion controlled. The slopes of the linear fits—and thereby the related diffusion coefficients—in both steps decrease in the following order of MOF-808-1.5*x*AQ, MOF-808, and MOF-808-3*x*AQ (Figure S19). This result supports our theory regarding the combined effect of AQ loading and pore volume on ion diffusion. Although possessing more redox-active sites within the MOF matrix, MOF-808-3*x*AQ loses around 50% of its pore volume in comparison to the pristine MOF-808. The insufficient pore space cancels out the positive impact of AQ incorporation on ion diffusion in this case. In contrast, MOF-808-1.5*x*AQ balances between the AQ loading and pore volume, presenting the best diffusion behavior of the three samples.

To investigate the impact of ion diffusion on cycling behavior in the MOF-808 series, MOF-808+S and MOF-808-*x*AQ+S composite cathodes were galvanostatically cycled at various *C* rates. MOF-808-1.5*x*AQ+S composites exhibit highest specific capacity at all *C* rates. When tested for long-term cycling at *C*/2 (Figure 5c), MOF-808-1.5*x*AQ+S composites deliver an average capacity of 716 mAh g^{-1} at the 100th cycle, while MOF-808-3*x*AQ+S composites and MOF-808+S composites deliver 561 and 513 mAh g^{-1}, respectively. The flat decay trend of MOF-808-AQ+S indicates these cells have high cyclability. When cycled for rate capability (Figure 5d and Figure S20), MOF-808-1.5*x*AQ+S composites also exhibit much enhanced specific capacity, demonstrating their impressive sulfur utilization and cyclability even at high *C* rates. Interestingly, MOF-808-3*x*AQ+S composites only show slight improvement over MOF-808+S composites at *C*/2, while almost no improvement at 1*C* and higher as pore space availability becomes increasingly crucial for fast charge transfer. These cycling results along with the galvanostatic profiles (Figures S21 and S22) of MOF-808-*x*AQ+S composites further illustrate that the electrochemical performance does not enhance monotonically with the AQ amount.

EIS of cells at their discharged state after cycling (Figure S23) was also analyzed to understand the combined effects of AQ loading and pore volume on electrokinetics. As shown in Table S6, electrolyte resistance, electrode surface resistance, and charge transfer resistance of the MOF-808-1.5*x*AQ+S cell are lower than that of the MOF-808+S cell, which is an indication of less polysulfide leaching and more favorable redox

https://dx.doi.org/10.1021/acs.chemmater.0c02438
Chem. Mater. 2020, 32, 8450−8459

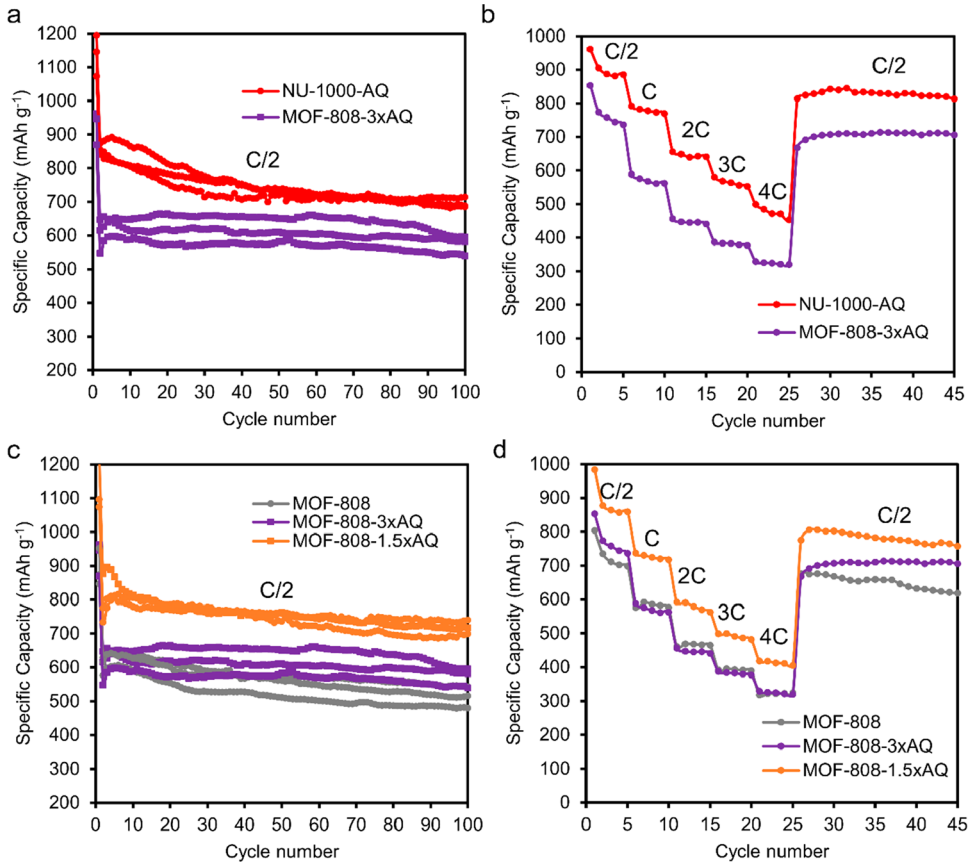

Figure 5. Porosity effect on electrochemical performance. Galvanostatic cycling results of (a, b) NU-1000-AQ and MOF-808-3*x*AQ and (c, d) MOF-808, MOF-808-1.5*x*AQ, and MOF-808-3*x*AQ at various *C* rates. Triplicate cells are shown for (a) and (c). Cell performance for MOF-808-3*x*AQ+S is duplicated in (a) and (c) and (b) and (d) for comparison.

kinetics. These parameters validate that introducing the proper amount of AQ into the MOF matrix without severely damaging its pore space can facilitate high sulfur utilization and improve cyclability at high *C* rates.

CONCLUSION

In summary, we took advantage of the unique postsynthetic tunability of metal−organic frameworks and introduced redox-activity to zirconium MOFs through open site functionalization with anthraquinone ligands. Utilizing these redox-active MOFs as cathode hosts in Li−S batteries, we observed the impact of AQ loading and porosity on capacity delivery and retention at various *C* rates. With the outstanding rate capability and capacity retention of NU-1000-AQ host, we demonstrate the benefits of AQ incorporation to achieve enhanced charge transfer and polysulfide encapsulation in Li−S cycling. The importance of balancing between AQ loading and available pore space was validated by the advantageous electrochemical behavior and performance of MOF-808-1.5*x*AQ over MOF-808-3*x*AQ. Our efforts provide insights into the structure−property−function relationship and motivate design strategies for porous frameworks with enhanced electrochemical ability to meet fast charge−discharge needs.

ASSOCIATED CONTENT

Supporting Information

The Supporting Information is available free of charge at https://pubs.acs.org/doi/10.1021/acs.chemmater.0c02438.

Additional thermogravimetric measurements, surface area analysis, UV−vis absorption spectra, and electrochemical measurements (PDF)

AUTHOR INFORMATION

Corresponding Author

V. Sara Thoi − *Department of Chemistry and Department of Materials Science and Engineering, Johns Hopkins University, Baltimore, Maryland 21218, United States;* orcid.org/0000-0003-0896-4077; Email: sarathoi@jhu.edu

Author

Bingqian Liu − *Department of Chemistry, Johns Hopkins University, Baltimore, Maryland 21218, United States*

Complete contact information is available at: https://pubs.acs.org/10.1021/acs.chemmater.0c02438

Notes

The authors declare no competing financial interest.

ACKNOWLEDGMENTS

We thank the National Science Foundation CAREER Award (DMR-1945114) as well as the Department of Chemistry and Johns Hopkins University (JHU) for instrumentation support, graduate student support, and start-up funding. We also acknowledge Prof. Tyrel McQueen (Dept. of Chemistry, JHU), Hector Vivanco (Dept. of Chemistry, JHU), and Nicholas Ng (Dept. of Chemistry, JHU) for PXRD assistance.

We thank Kevin Bennett (Dept. of Chemistry, JHU) for discussion and editing of this manuscript.

REFERENCES

(1) Mehtab, T.; Yasin, G.; Arif, M.; Shakeel, M.; Korai, R. M.; Nadeem, M.; Muhammad, N.; Lu, X. Metal-Organic Frameworks for Energy Storage Devices: Batteries and Supercapacitors. *J. Energy Storage* **2019**, *21*, 632−646.

(2) Xu, G.; Nie, P.; Dou, H.; Ding, B.; Li, L.; Zhang, X. Exploring Metal Organic Frameworks for Energy Storage in Batteries and Supercapacitors. In *Materials Today*; Elsevier B.V.: 2017; pp 191−209.

(3) Baumann, A. E.; Burns, D. A.; Liu, B.; Thoi, V. S. Metal-Organic Framework Functionalization and Design Strategies for Advanced Electrochemical Energy Storage Devices. In *Communications Chemistry*; Springer Nature: 2019; pp 1−14.

(4) Wu, H. B.; Lou, X. W. Metal-Organic Frameworks and Their Derived Materials for Electrochemical Energy Storage and Conversion: Promises and Challenges. *Sci. Adv.* **2017**, *3*, eaap9252.

(5) Wang, D.-W.; Zeng, Q.; Zhou, G.; Yin, L.; Li, F.; Cheng, H.-M.; Gentle, I. R.; Lu, G. Q. M. Carbon−Sulfur Composites for Li−S Batteries: Status and Prospects. *J. Mater. Chem. A* **2013**, *1* (33), 9382.

(6) Bruce, P. G.; Freunberger, S. A.; Hardwick, L. J.; Tarascon, J.-M. Li−O2 and Li−S Batteries with High Energy Storage. *Nat. Mater.* **2012**, *11* (1), 19−29.

(7) Rosenman, A.; Markevich, E.; Salitra, G.; Aurbach, D.; Garsuch, A.; Chesneau, F. F. Review on Li-Sulfur Battery Systems: An Integral Perspective. *Adv. Energy Mater.* **2015**, *5* (16), 1500212.

(8) Fang, R.; Zhao, S.; Sun, Z.; Wang, D.-W.; Cheng, H.-M.; Li, F. More Reliable Lithium-Sulfur Batteries: Status, Solutions and Prospects. *Adv. Mater.* **2017**, *29* (48), 1606823.

(9) Jiang, H.; Liu, X.-C.; Wu, Y.; Shu, Y.; Gong, X.; Ke, F.-S.; Deng, H. Metal-Organic Frameworks for High Charge-Discharge Rates in Lithium-Sulfur Batteries. *Angew. Chem., Int. Ed.* **2018**, *57* (15), 3916−3921.

(10) Zheng, J.; Tian, J.; Wu, D.; Gu, M.; Xu, W.; Wang, C.; Gao, F.; Engelhard, M. H.; Zhang, J.-G.; Liu, J.; et al. Lewis Acid−Base Interactions between Polysulfides and Metal Organic Framework in Lithium Sulfur Batteries. *Nano Lett.* **2014**, *14* (5), 2345−2352.

(11) Sun, L.; Campbell, M. G.; Dincă, M. Electrically Conductive Porous Metal-Organic Frameworks. *Angew. Chem., Int. Ed.* **2016**, *55* (11), 3566−3579.

(12) Zheng, Y.; Zheng, S.; Xue, H.; Pang, H. Metal-Organic Frameworks for Lithium-Sulfur Batteries. *J. Mater. Chem. A* **2019**, *7*, 3469−3491.

(13) Wu, Y.; Jiang, H.; Ke, F.; Deng, H. Three-Dimensional Hierarchical Constructs of MOF-on-Reduced Graphene Oxide for Lithium−Sulfur Batteries. *Chem. - Asian J.* **2019**, *14* (20), 3577−3582.

(14) Hong, J. Y.; Jung, Y.; Park, D. W.; Chung, S.; Kim, S. Synthesis and Electrochemical Analysis of Electrode Prepared from Zeolitic Imidazolate Framework (ZIF)-67/Graphene Composite for Lithium Sulfur Cells. *Electrochim. Acta* **2018**, *259*, 1021−1029.

(15) Zhang, H.; Zhao, W.; Zou, M.; Wang, Y.; Chen, Y.; Xu, L.; Wu, H.; Cao, A. 3D, Mutually Embedded MOF@Carbon Nanotube Hybrid Networks for High-Performance Lithium-Sulfur Batteries. *Adv. Energy Mater.* **2018**, *8* (19), 1800013.

(16) Hou, Y.; Mao, H.; Xu, L. MIL-100(V) and MIL-100(V)/RGO with Various Valence States of Vanadium Ions as Sulfur Cathode Hosts for Lithium-Sulfur Batteries. *Nano Res.* **2017**, *10* (1), 344−353.

(17) Calbo, J.; Golomb, M. J.; Walsh, A. Redox-Active Metal-Organic Frameworks for Energy Conversion and Storage. *J. Mater. Chem. A* **2019**, *7*, 16571−16597.

(18) D'Alessandro, D. M. Exploiting Redox Activity in Metal-Organic Frameworks: Concepts, Trends and Perspectives. *Chem. Commun.* **2016**, *52* (58), 8957−8971.

(19) Xiao, D. J.; Oktawiec, J.; Milner, P. J.; Long, J. R. Pore Environment Effects on Catalytic Cyclohexane Oxidation in Expanded Fe2(Dobdc) Analogues. *J. Am. Chem. Soc.* **2016**, *138* (43), 14371−14379.

(20) Tian, B.; Ning, G. H.; Gao, Q.; Tan, L. M.; Tang, W.; Chen, Z.; Su, C.; Loh, K. P. Crystal Engineering of Naphthalenediimide-Based Metal-Organic Frameworks: Structure-Dependent Lithium Storage. *ACS Appl. Mater. Interfaces* **2016**, *8* (45), 31067−31075.

(21) Park, S. S.; Hontz, E. R.; Sun, L.; Hendon, C. H.; Walsh, A.; Van Voorhis, T.; Dincă, M. Cation-Dependent Intrinsic Electrical Conductivity in Isostructural Tetrathiafulvalene-Based Microporous Metal-Organic Frameworks. *J. Am. Chem. Soc.* **2015**, *137* (5), 1774−1777.

(22) Hod, I.; Bury, W.; Gardner, D. M.; Deria, P.; Roznyatovskiy, V.; Wasielewski, M. R.; Farha, O. K.; Hupp, J. T. Bias-Switchable Permselectivity and Redox Catalytic Activity of a Ferrocene-Functionalized, Thin-Film Metal-Organic Framework Compound. *J. Phys. Chem. Lett.* **2015**, *6* (4), 586−591.

(23) Zhang, Y.; Riduan, S. N.; Wang, J. Redox Active Metal- and Covalent Organic Frameworks for Energy Storage: Balancing Porosity and Electrical Conductivity. *Chem. - Eur. J.* **2017**, *23* (65), 16419−16431.

(24) Lin, S.; Usov, P. M.; Morris, A. J. The Role of Redox Hopping in Metal-Organic Framework Electrocatalysis. *Chem. Commun.* **2018**, *54* (51), 6965−6974.

(25) Cai, M.; Loague, Q.; Morris, A. J. Design Rules for Efficient Charge Transfer in Metal-Organic Framework Films: The Pore Size Effect. *J. Phys. Chem. Lett.* **2020**, *11* (3), 702−709.

(26) Celis-Salazar, P. J.; Cai, M.; Cucinell, C. A.; Ahrenholtz, S. R.; Epley, C. C.; Usov, P. M.; Morris, A. J. Independent Quantification of Electron and Ion Diffusion in Metallocene-Doped Metal-Organic Frameworks Thin Films. *J. Am. Chem. Soc.* **2019**, *141* (30), 11947−11953.

(27) Mohammad-Pour, G. S.; Hatfield, K. O.; Fairchild, D. C.; Hernandez-Burgos, K.; Rodríguez-López, J.; Uribe-Romo, F. J. A Solid-Solution Approach for Redox Active Metal-Organic Frameworks with Tunable Redox Conductivity. *J. Am. Chem. Soc.* **2019**, *141* (51), 19978−19982.

(28) Palmer, R. H.; Liu, J.; Kung, C. W.; Hod, I.; Farha, O. K.; Hupp, J. T. Electroactive Ferrocene at or near the Surface of Metal-Organic Framework UiO-66. *Langmuir* **2018**, *34* (16), 4707−4714.

(29) Hod, I.; Farha, O. K.; Hupp, J. T. Modulating the Rate of Charge Transport in a Metal-Organic Framework Thin Film Using Host:Guest Chemistry. *Chem. Commun.* **2016**, *52* (8), 1705−1708.

(30) Halls, J. E.; Hernán-Gómez, A.; Burrows, A. D.; Marken, F. Metal-Organic Frameworks Post-Synthetically Modified with Ferrocenyl Groups: Framework Effects on Redox Processes and Surface Conduction. *Dalt. Trans.* **2012**, *41* (5), 1475−1480.

(31) Bai, Y.; Dou, Y.; Xie, L. H.; Rutledge, W.; Li, J. R.; Zhou, H. C. Zr-Based Metal-Organic Frameworks: Design, Synthesis, Structure, and Applications. *Chem. Soc. Rev.* **2016**, *45*, 2327−2367.

(32) Zhang, Z.; Yoshikawa, H.; Awaga, K. Discovery of a "Bipolar Charging" Mechanism in the Solid-State Electrochemical Process of a Flexible Metal-Organic Framework. *Chem. Mater.* **2016**, *28* (5), 1298−1303.

(33) Zhang, Z.; Yoshikawa, H.; Awaga, K. Monitoring the Solid-State Electrochemistry of Cu(2,7-AQDC) (AQDC = Anthraquinone Dicarboxylate) in a Lithium Battery: Coexistence of Metal and Ligand Redox Activities in a Metal-Organic Framework. *J. Am. Chem. Soc.* **2014**, *136* (46), 16112−16115.

(34) Liu, B.; Baumann, A. E.; Thoi, V. S. Modulating Charge Transport in MOFs with Zirconium Oxide Nodes and Redox-Active Linkers for Lithium Sulfur Batteries. *Polyhedron* **2019**, *170*, 788−795.

(35) Islamoglu, T.; Otake, K. I.; Li, P.; Buru, C. T.; Peters, A. W.; Akpinar, I.; Garibay, S. J.; Farha, O. K. Revisiting the Structural Homogeneity of NU-1000, a Zr-Based Metal-Organic Framework. *CrystEngComm* **2018**, *20* (39), 5913−5918.

(36) Deria, P.; Bury, W.; Hod, I.; Kung, C. W.; Karagiaridi, O.; Hupp, J. T.; Farha, O. K. MOF Functionalization via Solvent-Assisted Ligand Incorporation: Phosphonates vs Carboxylates. *Inorg. Chem.* **2015**, *54* (5), 2185−2192.

(37) Furukawa, H.; Gándara, F.; Zhang, Y. B.; Jiang, J.; Queen, W. L.; Hudson, M. R.; Yaghi, O. M. Water Adsorption in Porous Metal-

Organic Frameworks and Related Materials. *J. Am. Chem. Soc.* **2014**, *136* (11), 4369−4381.
(38) Kolosnitsyn, V. S.; Kuzmina, E. V.; Karaseva, E. V.; Mochalov, S. E. A Study of the Electrochemical Processes in Lithium-Sulphur Cells by Impedance Spectroscopy. *J. Power Sources* **2011**, *196* (3), 1478−1482.
(39) Morris, W.; Wang, S.; Cho, D.; Auyeung, E.; Li, P.; Farha, O. K.; Mirkin, C. A. Role of Modulators in Controlling the Colloidal Stability and Polydispersity of the UiO-66 Metal-Organic Framework. *ACS Appl. Mater. Interfaces* **2017**, *9* (39), 33413−33418.
(40) Ali, N. W.; Abdelwahab, N. S.; Abdelkawy, M.; Emam, A. A. Validated Stability Indicating TLC-Densitometric Method for the Determination of Diacerein. *J. Chromatogr. Sci.* **2014**, *52* (1), 5−11.
(41) Yang, F.; Li, W.; Tang, B. Facile Synthesis of Amorphous UiO-66 (Zr-MOF) for Supercapacitor Application. *J. Alloys Compd.* **2018**, *733*, 8−14.
(42) Wang, W.; Xu, W.; Cosimbescu, L.; Choi, D.; Li, L.; Yang, Z. Anthraquinone with Tailored Structure for a Nonaqueous Metal-Organic Redox Flow Battery. *Chem. Commun.* **2012**, *48* (53), 6669−6671.
(43) Park, H.; Siegel, D. J. Tuning the Adsorption of Polysulfides in Lithium-Sulfur Batteries with Metal-Organic Frameworks. *Chem. Mater.* **2017**, *29* (11), 4932−4939.
(44) Baumann, A. E.; Burns, D. A.; Díaz, J. C.; Thoi, V. S. Lithiated Defect Sites in Zr Metal-Organic Framework for Enhanced Sulfur Utilization in Li-S Batteries. *ACS Appl. Mater. Interfaces* **2019**, *11* (2), 2159−2167.
(45) Liang, Y.; Hui, J. K. -H.; Yamada, T.; Kimizuka, N. Electrochemical Thermoelectric Conversion with Polysulfide as Redox Species. *ChemSusChem* **2019**, *12* (17), 4014−4020.
(46) Bieker, G.; Diddens, D.; Kolek, M.; Borodin, O.; Winter, M.; Bieker, P.; Jalkanen, K. Cation-Dependent Electrochemistry of Polysulfides in Lithium and Magnesium Electrolyte Solutions. *J. Phys. Chem. C* **2018**, *122* (38), 21770−21783.
(47) Bard, A. J.; Faulkner, L. R. *Electrochemical Methods: Fundmanentals and Applications*, 2nd ed.; John Wiley & Sons, Inc.: New York, 2001.

https://dx.doi.org/10.1021/acs.chemmater.0c02438
Chem. Mater. 2020, 32, 8450−8459